INTERNATIONAL JOURNAL OF CLIMATOLOGY
Int. J. Climatol. **38** (Suppl.1): e554–e568 (2018)
Published online 22 December 2017 in Wiley Online Library
(wileyonlinelibrary.com) DOI: 10.1002/joc.5389

Attributing drivers of the 2016 Kenyan drought

Peter Uhe,[a,b*,†] Sjoukje Philip,[c] Sarah Kew,[c] Kasturi Shah,[d] Joyce Kimutai,[e] Emmah Mwangi,[e] Geert Jan van Oldenborgh,[c] Roop Singh,[f] Julie Arrighi,[f] Eddie Jjemba,[f] Heidi Cullen[d] and Friederike Otto[a]

[a] *Environmental Change Institute, University of Oxford, UK*
[b] *Oxford e-Research Centre, University of Oxford, UK*
[c] *Royal Netherlands Meteorological Institute (KNMI), De Bilt, The Netherlands*
[d] *Climate Central, Princeton, NJ, USA*
[e] *Kenya Meteorological Department, Nairobi, Kenya*
[f] *Red Cross Red Crescent Climate Centre, The Hague, The Netherlands*

ABSTRACT: In 2016 and continuing into 2017, Kenya experienced drought conditions, with over 3 million people in need of food aid due to low rainfall during 2016. Whenever extreme events like this happen, questions are raised about the role of climate change and how natural variability such as the El Niño - Southern Oscillation influenced the likelihood and intensity of the event. Here we aim to quantify the relative contributions of different climate drivers to this drought by applying three independent methodologies of extreme event attribution. Analysing precipitation data for the South East and North West of Kenya we found no consistent signal from human-induced climate change and thus conclude that it has not greatly affected the likelihood of low rainfall such as in 2016. However, 2016 was a La Niña year and we show that this event was indeed more likely because of the specific sea surface temperatures. There is a trend in temperatures in the region due to climate change that may have exacerbated the effects of this drought. By analysing precipitation minus evaporation and soil moisture, simulated by one climate model only, we did not see a reduction in moisture in simulations in the current climate compared with simulations without climate change. However, there are expected effects of higher temperatures that our simulations do not cover, such as increased demand on water resources and stress on livestock. Although we find no significant influence of climate change on precipitation, we cannot rule out that temperature-related impacts of drought are linked to human-induced climate change.

KEY WORDS attribution; climate change; drought; El Niño; Kenya

Received 4 April 2017; Revised 23 November 2017; Accepted 24 November 2017

1. Introduction

At the beginning of 2017, much of Kenya was suffering the effects of the low rainfall and high temperatures that occurred in 2016. By January, 2.6 million people in Kenya were in need of food aid according to a report conducted by the Kenya Food Security Steering Group (KFSSG, 2017), rising to over 3 million in March. The Kenyan National Drought Management Authority had declared alarm stage in 15 counties, and alert stage in 7 counties (NDMA, 2017). In March 2017, the Kenyan government declared the drought a National Emergency.

This is not the first time reduced rainfall has resulted in a crisis in Kenya. The deadly 2010–2011 La Niña-driven drought is still fresh in the minds of many East Africans. The Kenyan NDMA was established following the 2010–2011 drought to ensure a coordinated effort to manage drought risk in the future.

Kenya is highly vulnerable to drought. Most of the country (over 80%) is characterized as arid or semi-arid lands, with annual rainfall less than 550 or 850 mm, respectively. Under this definition, the arid and semi-arid lands house the majority of all livestock in Kenya (70%) and around 30% of the population (Republic of Kenya, 2012). In addition to low rainfall, there is a wide range of year-to-year variability in rainfall (see Section 2). For example, North West (NW) Kenya, an arid region, had 500 mm of rainfall in 1997 but only 150 mm in 2000. This variability in rainfall makes droughts a common occurrence. The areas analysed in this study, which were affected by the 2016 drought (NW and South East (SE) Kenya), are in arid or semi-arid regions.

The food insecurity in the current 2016–2017 drought was firstly attributable to the low rainfall in the October–December (OND) 2016 'short rains' (Figure 1(a)), particularly in the NW and the SE of Kenya. In addition to the lack of rain in the OND season, some areas including the SE were still dealing with the effects of low rainfall from the previous March–May (MAM) 2016 'long rains'. Accordingly, there is a large precipitation

* Correspondence to: P. Uhe, School of Geographical Sciences, University of Bristol, UK. E-mail: peter.uhe@bristol.ac.uk

† Present address: School of Geographical Sciences, University of Bristol, UK.

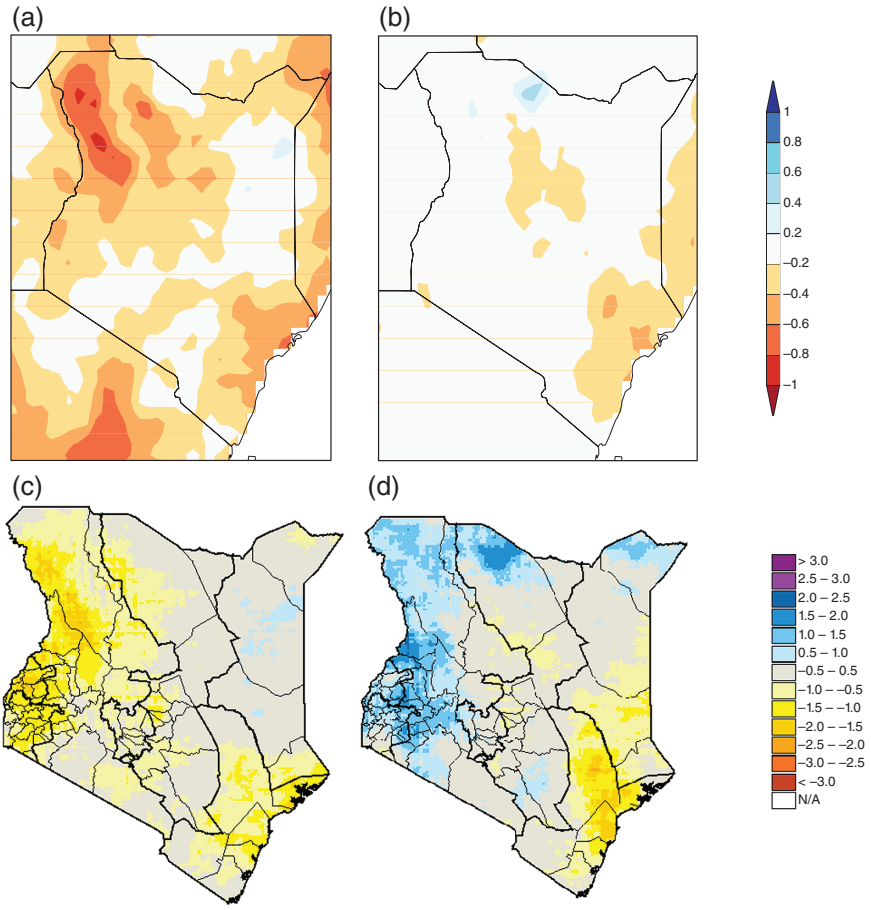

Figure 1. Spatial maps over Kenya for: (a) OND 2016 relative precipitation anomalies from the CHIRPS data set (anomalies with respect to 1986–2009), (b) January–December 2016 relative precipitation anomalies from the CHIRPS data set (anomalies with respect to 1986–2009), (c) SPI index calculated for OND 2016, and (d) SPI index calculated for MAM 2016. The SPI plots were calculated based on CHIRPS precipitation data using the GeoCLIM toolbox (https://earlywarning.usgs.gov/fews/software-tools/20).

deficit in the SE for the whole year (Figure 1(b)). A common way to look at the severity of a drought is the standardized precipitation index (SPI, McKee *et al.,* 1993), representing the cumulative probability of a rainfall event. The SPI for OND (Figure 1(c)) shows drought conditions in the NW and SE, and corresponds well with the precipitation anomaly in Figure 1(a). The SPI in MAM (Figure 1(d)) shows drought conditions in that season were limited to the SE, and were more severe than in the OND season in some regions. Other areas of East Africa, including Somalia and Ethiopia, were also experiencing drought conditions and food insecurity in early 2017, however, for this study we focus on the conditions in Kenya.

During 2016, starting in June and peaking in November, there was a strong La Niña event with a relative NINO3.4 index of −1.3 °C (this definition accounts for global warming, see Section 3 for details). La Niña is the negative phase of the El Niño - Southern Oscillation (ENSO). La Niña events have a negative correlation with OND rainfall in Kenya (Mutai and Ward, 2000; Nicholson and Selato, 2000). There was also a negative dipole mode index (DMI) during much of 2016. The DMI represents the Indian Ocean dipole (IOD), which is the difference between the sea surface temperatures (SSTs) in the western and eastern Indian Ocean (Saji *et al.,* 1999). The DMI is also correlated with OND East African rainfall, and a negative dipole results in reduced rainfall in the eastern sector of East Africa (Black *et al.,* 2003).

There is also a strong correlation between ENSO and the DMI, so it is difficult to separate their relative influences. However, it has been hypothesized that the East African rainfall is more closely connected to the IOD, and the influence of ENSO is manifested through its link with the IOD (Goddard and Graham, 1999; Black, 2005). IOD events may occur in connection with an El Niño event, but can be triggered independently from ENSO (Ashok *et al.,* 2003; Fischer *et al.,* 2005), so although in 2016 there were both negative ENSO and IOD events, this is not necessarily the case more generally. For instance, in 2011 there was a positive IOD index during La Niña, and above-average OND rainfall in Kenya.

Recent studies have also indicated that different patterns of the ENSO SST anomalies of the same phase can lead to significantly different teleconnections. Hoell *et al.* (2014) separated La Niña events into different phases and found that La Niña events characterized by cool central Pacific SSTs and warm west Pacific SSTs have a different

influence on the Indian Ocean and East African rainfall compared to the canonical east Pacific La Niña pattern (particularly in the MAM season). In addition, Preethi *et al.* (2015) compared the influence of the canonical El Niño, El Niño Modoki, and IOD on African rainfall. They found that El Niño Modoki and canonical El Niño have opposite impacts, resulting in below and above mean East African OND rainfall, respectively. ENSO clearly plays an important role with respect to drought risk in East Africa. However, the literature discussed shows that disentangling the role of Pacific SSTs and the influence of the Indian Ocean, as well as potential role of anthropogenic climate change is not straightforward and will likely not be uniform in time and space.

Previous studies on drought in Kenya have found differing results when analysing the effect of anthropogenic climate change. A number of studies have pointed out a drying trend of the long rains in East Africa in recent decades (e.g. Lyon and DeWitt, 2012) and there have been a number of studies discussing whether this is due to internal climate variability or forced by human-induced climate change. The drying trend is small compared to natural variability as noted by Yang *et al.* (2014), and this low signal to noise makes it difficult to attribute the cause of this trend, especially over a period as short as a few decades. This discussion has also been complicated by an increase in precipitation predicted by climate simulations. For example, Shongwe *et al.* (2011) used multi-model ensembles from global climate models (GCMs) to show the whole rainfall distribution in East Africa is positively shifted in a future climate: mean precipitation rates increase as does the intensity of high rainfall, and droughts become less severe. They describe physical mechanisms explaining this trend. However, they also stress that natural variability is so large that this trend will not become visible until well after the beginning of this century.

However, while GCMs show an increase in precipitation, atmospheric simulations forced by the observed patterns of SST variability can reproduce the recent drying of the long rains (Yang *et al.,* 2014; Hoell *et al.,* 2017). The SST patterns are a result of both natural and anthropogenic forcing, and using additional simulations, Hoell *et al.* (2017) indicated that the interaction of internal variability and anthropogenic forcing may have enhanced the drying trend compared to internal variability acting alone. Rowell *et al.* (2015) also examined a number of hypotheses for the drying trend not being present in coupled climate models, including changes to anthropogenic aerosols and inadequate representation of physics in climate models. They also determined that it was unlikely the drying trend could have resulted from natural variability alone. A mechanism of drying over East Africa was proposed by Liebmann *et al.* (2017), connecting increased convection over Indonesia to increased upper atmosphere easterly winds and lower rainfall in MAM, but did not separate the effect of anthropogenic forcing and natural variability.

Previous attribution studies have looked at the influence of human-induced climate change on specific droughts in East Africa. Lott *et al.* (2013) used event attribution methodologies on the 2010–2011 drought in Kenya and Somalia. They found that the 2010 short rains failed due to the La Niña event in 2010, however, human influence increased the probability of the dry 2011 long rains. In contrast, Marthews *et al.* (2015) found no anthropogenic influence on the likelihood of low rainfall in the long rains of 2014 in northern Kenya and southern Ethiopia, but human influences did increase temperatures and incoming ground surface radiation and thus the factors exacerbating the impacts of drought. We note that the results of these two studies for the long rains are not necessarily contradictory as they looked at different regions in East Africa and different years (both studies used SST-forced attribution), which may have different drivers of the drought. This indicates attribution results for a particular drought cannot be easily generalized to other droughts and highlights the importance of a case-based approach to an attribution analysis of individual events. It should also be noted that model dependencies are very large for drought attribution, as exemplified by the differing trends shown in Shongwe *et al.* (2011), and shown thoroughly for Europe in Hauser *et al.* (2017).

Another attribution study (Funk *et al.,* 2013) examined the ENSO-related SST effects rather than anthropogenic influence on the 2012 MAM rainfall deficit in eastern Kenya and southern Somalia. By repeating the analysis for the time periods 2003–2012 and 1993–2002 they found that while ENSO was a key driver of the dry spells in 1993–2002, effects other than ENSO contributed to the dry spells in the more recent 2003–2012 period. However, this may just reflect natural variability and the influence of the Indian Ocean independent of ENSO.

This study aims to investigate the respective contributions of anthropogenic climate change and large scale variability in SSTs for a specific case – the low rainfall over the OND season in NW Kenya and the yearly rainfall deficit in the SE Kenya. Focusing on a single OND season for the NW region allows us to more clearly examine possible connections with the Pacific and Indian Oceans. Analysing the whole year's rainfall in the SE can be linked to the accumulated impact of low rainfall for more than one season. The analysis is performed on observational data sets and multiple climate models with different experimental setups. Combining different approaches in this way, gives us a range of possible responses of this event to anthropogenic forcing and natural variability and hence greater confidence in the results.

For this study, we do not focus on the recent drying trend of the long rains, as we are investigating changes due to anthropogenic forcings in the order of a century rather than decades. The focus here is on the short rains and yearly rainfall rather than the long rains. There is not a significant drying trend reported in the short rains or yearly rainfall in the regions analysed in this study.

Section 2 describes the data products and models used; being observational data (Section 2.1), global climate models (Section 2.2), and large ensembles of regional climate models (Section 2.3). Section 3 then gives a brief description of the methods of analysis used and Section

4 gives an evaluation of the models against observations. We show our analysis of the low precipitation in Section 5, which is again broken up into analysis of observations (Sections 5.1 and 5.2), a comparison with the 2010–2011 drought (Section 5.3), analysis of the global climate models (Section 5.4) and the large ensembles of regional climate models (Section 5.5). In Section 6, we discuss other factors in the drought such as temperature, and look at the large ensembles of regional climate simulations to give an indication of the influence of climate change to available moisture (precipitation minus evaporation and also soil moisture).

2. Data and models

Different regions in Kenya have different rainfall characteristics, so we analyse a couple of smaller regions rather than the country as a whole. The areas of interest for this study are restricted to the regions in Kenya that had the most significant dry anomalies in 2016 (Figure 1). We label these the NW and SE (see Figure 2). The regions are defined by county boundaries to avoid selection bias in choosing specific regions for this analysis and to assist in making these regions relatable to people in Kenya. The NW region includes the counties Turkana and Marsabit, and the SE region includes Kwale, Kilifi, Mombasa, and Lamu.

Kenya has seasonal rainfall dominated by two rainy seasons: MAM and OND. The seasonal cycle of precipitation in the NW and SE are shown in Figures 3(a) and (b), respectively. There is high year to year variability, shown in the time-series of precipitation anomalies in Figures 3(c) and (d) and also the 95% range in Figures 3(a) and (b). The NW of Kenya is very dry with average rainfall of less than 1 mm day^{-1} for much of the year. In the year 2016 it was especially dry in OND (Figures 1(a) and 3(c)). Considering the SE of Kenya, the dry anomaly extended over both rainy seasons (Figures 1(b) and 3(d)).

For the NW region, we analyse the short rains only (OND), as this region had above average rainfall in the 2016 MAM rainy season and it is the rainfall deficit that is relevant to the drought's impact. In the SE, we consider the whole year from January to December 2016, as this captures the impact of below average rainfall for two consecutive rainy seasons.

2.1. Observational data

For observations, we use both station data and gridded data of monthly precipitation. The station data for the years 1981–2016 are provided by the Kenya Meteorological Department. These time series are extended back in time by the corresponding data sets in the monthly Global Historical Climatology Network station database (Peterson and Vose, 1997). We analyse two stations in the NW of Kenya for the OND season. These are Lodwar (3.10°N; 35.60°E, 515 m above sea level, 1920–2016) and Marsabit (2.00°N; 37.90°E, 1447 m above sea level, 1918–2016). The only station in the SE for which we have a long time series is Lamu (2.27°S; 40.90°E, 30 m above sea level, 1906–2016). We analyse the station data of Lamu for January–December 2016 but note that this station is not representative for the entire SE region.

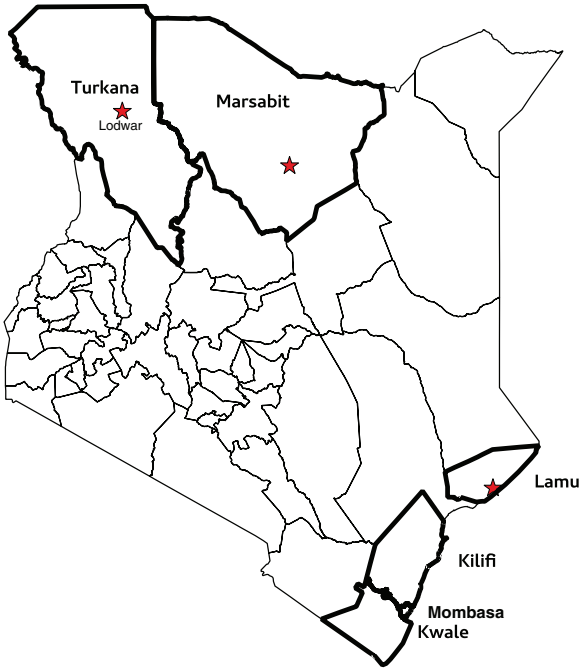

Figure 2. Map of Kenya highlighting the counties used in the analysis: NW includes Turkana and Marsabit and SE includes Kwale, Mombasa, Kilifi, and Lamu. Approximate location of the Marsabit, Lodwar, and Lamu stations are shown as stars.

The gridded data set is a combination of two data sets: CHIRPS (Climate Hazards Group InfraRed Precipitation with Station data; Funk *et al.,* 2015b) and CenTrends (Centennial Trends; Funk *et al.,* 2015a). CHIRPS is the state of the art observational daily dataset for East Africa for the years 1981–2016. CenTrends, on the other hand, is a monthly data set, available for 1900–2014. CenTrends and CHIRPS are based on a similar assimilation technique and underlying observational data for their overlap period. They are highly correlated, with correlations over 0.95, justifying the extension of the CenTrends data set with monthly averaged data from CHIRPS. A correction according to the regression between the two would result in no difference in the NW region and slightly higher precipitation values in the SE region. To avoid the introduction of extra errors we do not adjust this value, but bear in mind that return period in the SE region might be slightly overestimated. With the two data sets together, referred to as the CenTrends-ext data set, we can provide information about both the trend in the past and the current situation.

2.2. Global climate models

We analyse output from two global climate models (GCMs). The first GCM is EC-Earth (Hazeleger *et al.,* 2010) which is a coupled atmosphere–ocean model with a resolution of T159 (about 125 km over Kenya). The version used is EC-Earth 2.3, which is based on the European

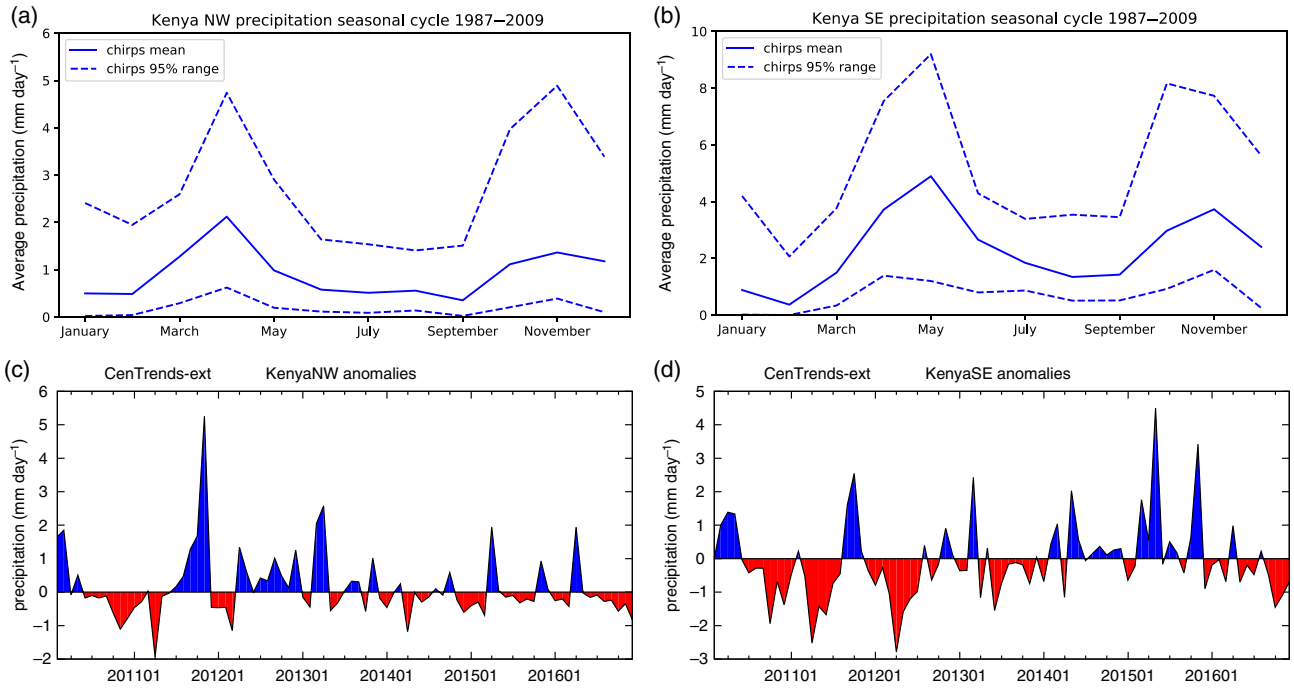

Figure 3. Seasonal cycle of CHIRPS monthly precipitation in: (a) NW Kenya from 1987 to 2009 and (b) SE Kenya from 1987 to 2009. For (a) and (b) the solid line is the mean precipitation and the dashed lines are the 95% range for each month, (c) time-series of precipitation anomalies over the past 7 years for the NW region, and (d) time-series of precipitation anomalies for the SE region. Blue/red means more/less than average precipitation (panels (c) and (d) show anomalies with respect to 1986–2009).

Centre for Medium-Range Weather Forecasts (ECMWF) seasonal forecasting model system 3 (Stockdale *et al.,* 2011). For EC-Earth, continuous simulations from 1860 to 2015 are used as per the CMIP5 historical setup until 2005 and the RCP8.5 scenario from 2006 (see Taylor *et al.,* 2012). The ensemble includes 16 members.

The second model used is UK Met Office model HadGEM3-A (Christidis *et al.,* 2013). In the EUropean CLimate Extremes Interpretation and Attribution (EUCLEIA) project, HadGEM3-A is an atmosphere-only model and was run with N216 horizontal resolution (about 60 km). These simulations are also part of the Climate of the Twentieth Century (C20C) Detection and Attribution project. For this model we have both historical simulations for 1960–2015, driven by observed SST, and historicalNat simulations (Taylor *et al.,* 2012) representing the historical period but with only non-anthropogenic forcings. The SST for these runs has been obtained by subtracting an estimate of the forced change in SST obtained from the mean CMIP5 ensemble response. As the runs for 2016 were not yet available at the time of writing, we used the trend up to 2015 as the indicator for the effects of natural and anthropogenic forcings.

2.3. Large ensemble regional climate modelling

To obtain an extensive sample of possible weather under different scenarios, we make use of the large ensemble distributed computing framework of weather@home (Massey *et al.,* 2015). This uses the Met Office Hadley Centre regional atmospheric circulation model HadRM3P, at 50-km resolution over Africa, nested in the global atmosphere-only model HadAM3P. With this model, thousands of simulations are run for two scenarios: Actual and Natural. The Actual simulations use current greenhouse gas (GHG) and aerosol concentrations, and observed SSTs and sea-ice extent from the OSTIA data set (Donlon *et al.,* 2012). The Natural simulations use preindustrial levels of GHGs, multiple anthropogenic warming patterns subtracted from the OSTIA SSTs (as per Schaller *et al.,* 2016) and the maximum observed sea-ice extent in the OSTIA data set. In addition to simulations of 2016, we have a reference data set of Actual simulations from 1987 to 2009 (referred to as Climatology).

Different simulations were produced by varying the initial conditions. Forty starting conditions from previous simulations were used in each scenario and different initial condition perturbations were applied to the potential temperature to obtain thousands of unique initial conditions, producing different simulations of possible weather. A larger number of simulations were computed covering just OND 2016, than were computed for the whole year of 2016, due to computational constraints. The number of ensemble members for each of the scenarios are: Actual: 3474 for OND and 2536 for January–December; Natural: 7003 for OND and 4285 for January–December; and Climatology: 3596.

3. Methods

We used statistical methods to analyse the precipitation in the NW and SE regions of Kenya. As mentioned above, we considered precipitation from the observational data

sets CHIRPS, CenTrends and observations from stations in Marsabit, Lamu, and Lodwar. The GCMs are EC-Earth version 2.3 and HadGEM3-A, and the regional climate model is weather@home.

In order to determine the return times of the low precipitation values we fit the low tail of the observed and modelled precipitation distributions to a generalized Pareto distribution (GPD, Coles, 2001), which has a cumulative distribution H:

$$H(x-\mu) = 1 - \left(1 - \frac{\xi(x-\mu)}{\sigma}\right)^{(-1/\xi)} \quad (1)$$

where μ is the threshold, in this case chosen so that the lowest 20% of data points are fitted, σ is the scale parameter, and ξ is the shape parameter. To allow for a trend in probability the threshold and shape parameters are dependent on the 4-year running mean of global mean temperature (T, also referred to as smoothed GMST) with a trend α such that their ratio is constant and with an exponential dependence that scales the whole PDF:

$$\mu = \mu_0 \ \exp\left(\frac{\alpha T}{\mu_0}\right)$$

$$\sigma = \sigma_0 \ \exp\left(\frac{\alpha T}{\mu_0}\right)$$

The trend α is fitted together with the other parameters in a maximum likelihood procedure. The fit is constrained to have zero probability below zero precipitation ($\xi < 0$, $\sigma < \mu\xi$). Unphysically large shape parameters are suppressed by a penalty term that keeps them roughly in the range $|\xi| < 0.4$ (as per Schaller *et al.,* 2014; van der Wiel *et al.,* 2017).

When calculating the distribution, the value of the year of interest is not used in the fit. As the GPD includes a covariate (smoothed GMST) that varies with time, we can evaluate the precipitation distribution for a given year (for this study, 1920, and 2016). The precipitation series are also shown twice, scaled with the fitted trend to 2016 and 1920 GMST values. The difference in the two distributions shows whether there is a trend, with the uncertainty range estimated with a 1000-member nonparametric bootstrap. This takes into account dependencies between ensemble members of SST-forced models with a moving block technique.

The EC-Earth and HadGEM3-A models are analysed using the same method as for the observations, calculating the return times and trend from the GPD fit. These models have multiple long climate simulations, which reduces the statistical uncertainty shown in the confidence interval bounds, compared to the observations. The models have an additional structural uncertainty due to how the models represent climate processes and this is not included in the uncertainty estimates quoted in for each model. However, the spread across the different models, with different representations of the physics, gives an idea of this structural uncertainty.

For the weather@home data, we take advantage of the thousands of simulations to describe the distribution of possible weather under different climate conditions, and do not fit an extreme value distribution to determine return periods. The sampling uncertainty of return periods in weather@home data is calculated by randomly resampling the distribution 1000 times. Again we note that this uncertainty represents the variability in the model, but not the structural uncertainty due to model physics. Hence a small uncertainty range does not indicate confidence in the results but indicates that the type of event is well sampled using this methodology. Comparisons with the other methods are necessary to assess confidence in results. For this study we do not bias correct the weather@home data. Therefore, we use a threshold based on the observed return period, instead of the observed magnitude of the event which would first require the data to be bias corrected.

In the gridded observational data sets we also analyse the role of ENSO in this drought. As the teleconnection to East African rainfall is related to the ENSO variability and not to the trend, a detrended NINO3.4 index is used for this analysis, see Philip *et al.* (2017) and van Oldenborgh *et al.* (submitted). The detrended NINO3.4 index is defined in this study as SST in the NINO3.4 region (5°S–5°N, 120–170°W) minus SST averaged of 30°S–30°N to remove to first-order effects of global warming from the index. Detrending in this manner is preferable to a linear detrending of the index itself, as the warming signal is nonlinear. The 30°S–30°N region was chosen to represent tropical SSTs as the difference in NINO3.4 temperature and the wider tropical region is important for ENSO. Correlations between monthly precipitation and the NINO3.4 index of the same month are calculated. We then subtract a linear approximation of the influence of ENSO from the observational data for each month in the 2016 event. This allows us to calculate the return time for a hypothetical event for 2016 as if it had happened under ENSO-neutral conditions. In order to keep the precipitation values above zero we apply a logarithmic transformation on the precipitation before subtracting the influence of NINO3.4.

We also look at correlations of the Kenyan precipitation and Indian Ocean SSTs, represented by the DMI. The DMI is comprised of the difference between the western Indian Ocean (WIO) SSTs, 10°S–10°N, 50–70°E, and the south eastern Indian Ocean SSTs, 10–0°S, 90–110°E. The DMI is not detrended as per NINO3.4 as it represents a difference or gradient in the Indian Ocean SSTs. The WIO index (detrended by subtracting the influence of change in GMST) is also considered as a separate index.

4. Evaluation of model precipitation

The gridded CenTrends-ext precipitation data is more comparable to the model data than the station data so is used to evaluate the model precipitation distributions. For precipitation in NW Kenya in October–December and SE Kenya in January–December, the GPD fit of the CenTrends-ext data gives a good description of the dry tail.

Table 1. GPD fit parameters for EC-Earth and HadGEM3-A, compared against CenTrends-ext.

	σ/μ	ξ	Bias correction factor
NW Kenya (October–December)			
CenTrends-ext	0.25 (0.14, 0.31)	−0.25 (−0.33, −0.15)	
EC-Earth	0.34 (0.30, 0.38)	−0.41 (−0.49, −0.34)	1.15
HadGEM3-A	0.19 (0.16, 0.23)	−0.24 (−0.38, −0.17)	1.33
SE Kenya (January–December)			
CenTrends-ext	0.09 (0.05, 0.13)	−0.10 (−0.23, −0.06)	
EC-Earth	0.11 (0.10, 0.14)	−0.14 (−0.26, −0.13)	0.83
HadGEM3-A	0.10 (0.08, 0.11)	−0.23 (−0.35, −0.09)	1.18

The parameters used for validation are the ratio of parameters σ/μ (scale and location parameters) and ξ (shape parameter). Uncertainty ranges for the parameters are shown in brackets. The bias correction factor calculated from the data is also shown.

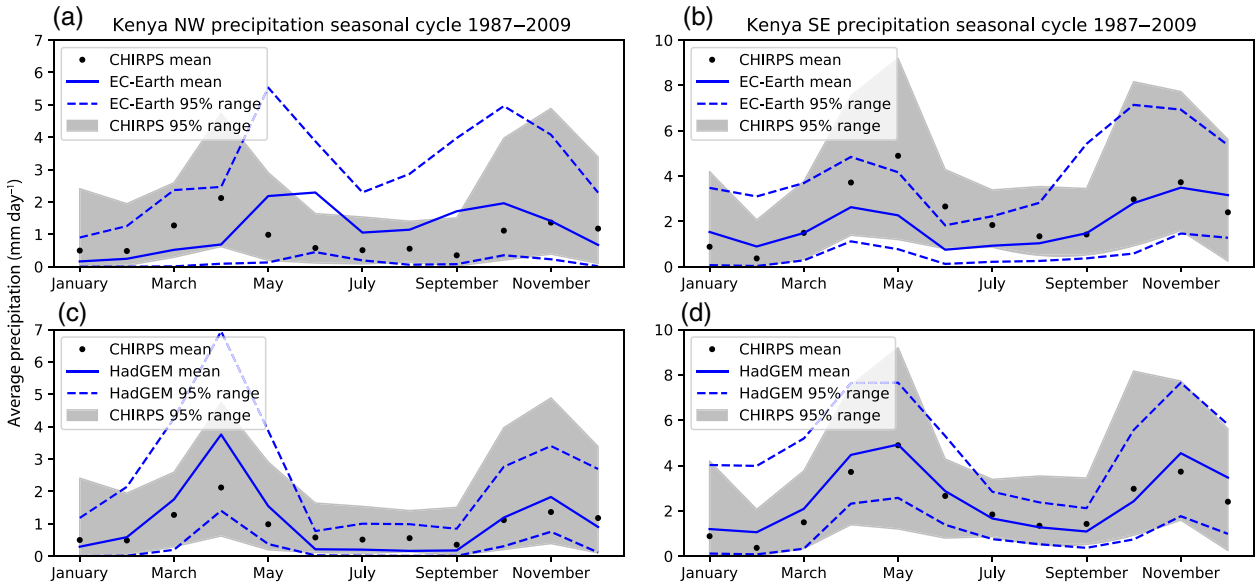

Figure 4. Seasonal cycles of precipitation for 1987–2009: (a) EC-Earth in NW Kenya, (b) EC-Earth in SE Kenya, (c) HadGEM3-A in NW Kenya, and (d) HadGEM3-A in SE Kenya. Solid line shows the monthly mean precipitation and the dashed lines show the 95% range of monthly precipitation. CHIRPS data shown for comparison – dots are the CHIRPS monthly mean and shaded area is the 95% range of monthly precipitation in CHIRPS.

The GPD fits of the monthly precipitation from the EC-Earth and HadGEM3-A models were validated against the fits for the CenTrends-ext precipitation distributions, see Table 1. This table also includes the multiplicative bias correction factor. The seasonal cycles for the models in each region are also shown in Figure 4. The parameters validated are the ratio of σ and μ (as it is assumed that the scale parameter σ scales with the position parameter μ), and also the shape parameter ξ. If the model parameters are within the uncertainty bounds of the fit parameters in observations we consider this model for analysis and employ a multiplicative bias correction for the model value in 2016 if necessary.

The GPD fit parameters, σ/μ and ξ, of the EC-Earth precipitation time series in the NW region, are respectively just within and just outside the confidence margins of the fit parameters given from observations. We include the EC-Earth results for this region but keep in mind that this is at the edge of the plausible range of distributions. The fit parameters for the SE region are well within the confidence margins from observations, so we trust this result, although we have to remark that this region contains only three grid boxes in this model. We also note that from Figure 4(a), the short rains start earlier than the observations in NW Kenya. The seasonal cycle is represented better in the SE, although with an underestimation of rainfall during the long rains (Figure 4(b)).

A statistical model evaluation of HadGEM3-A monthly precipitation in the NW region shows that the fit parameters of the time series are within the uncertainty range of the parameters fitted from observations, so we include this model in our analysis. The seasonal cycle is represented well (Figure 4(c)), and as the historicalNat runs do not show a trend over the whole period, this gives us greater confidence in the trend of the historical runs.

In the SE region the situation is more complicated. The fit parameters of the time series of SE Kenya precipitation for HadGEM3-A in January–December are within the uncertainty range of the parameters of the observational distribution, and the seasonal cycle of rainfall is represented well (Figure 4(d)). However, the historicalNat runs have a strong significant trend towards drier conditions. The 2016 low rainfall was 33 times more likely to occur in 2016 than in 1920, based on the historicalNat

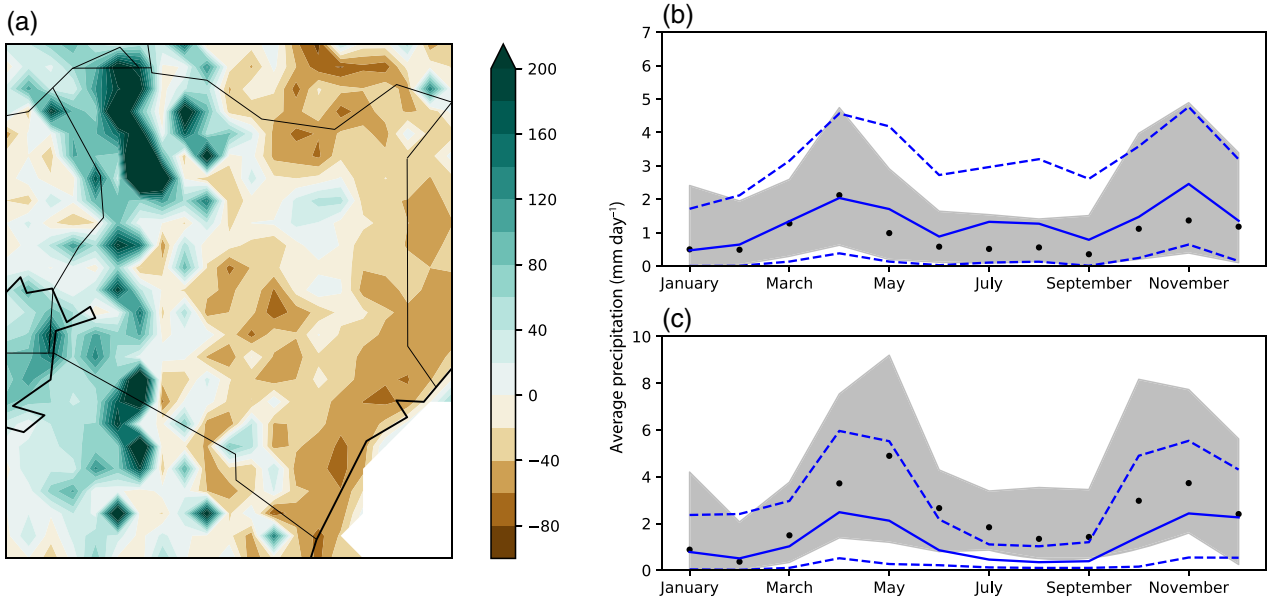

Figure 5. (a) Map of climatological yearly precipitation bias over Kenya for weather@home. The bias is relative to CHIRPS over the 1987–2009 period and expressed in percent. (b) and (c) are seasonal cycles of weather@home precipitation for 1987–2009; (b) in NW Keyna and (c) in SE Kenya. Solid line shows the monthly mean precipitation and the dashed lines show the 95% range of monthly precipitation. CHIRPS data shown for comparison: dots are the CHIRPS monthly mean and shaded area is the 95% range of monthly precipitation in CHIRPS.

trend. To compare, the trend in the historical simulations is about half of that (the 2016 event was 14 times more likely to occur in 2016 than in 1920). Using a linear subtraction of the two trends indicates a wetting trend due to anthropogenic influences. However, as the model drift is relatively large, we do not trust this linear subtraction and do not consider this model further for the SE region.

Comparing the weather@home climatology to the CHIRPS data set, the weather@home model does have biases in rainfall, see Figure 5(a). The NW region has a wet bias in the short rains (OND) of 0.8 mm day^{-1}. As this region is particularly dry, this is a large percentage bias relative to CHIRPS (75%). The SE has a dry bias in the annual mean (−1.3 mm day^{-1}) which is 51% drier than CHIRPS. Because of this, we do not estimate return times from the absolute precipitation values in the model. However, we note that despite the absolute magnitude of rainfall not being well captured, the model does replicate the seasonal cycle reasonably well (Figures 5(b) and (c)). During OND in the NW, the weather@home precipitation matches the spread of precipitation in the CHIRPS data set despite the average being too high. In addition, the year to year variability of the weather@home OND rainfall, forced by SSTs, shows a similar response to the observations in both regions. For the weather@home analysis, the return periods from the CenTrends-ext data set were used as the threshold for the 2016 event.

5. Precipitation analysis

5.1. Return times in station observations

The data for the precipitation stations at Marsabit in the NW and Lamu in the SE are shown in Figure 6. Results for Lodwar are not shown, as this time series did not fit a GPD properly and we were not able to calculate a return time. Probably this is because this station is so dry that it happens more often than not that there is hardly any precipitation. It is very difficult to estimate the return time of a value of almost zero. For the remaining two stations, the data are plotted against the covariate used in the GPD fits (smoothed GMST), showing the trends in the data (Figures 6(a) and (b)). Return time plots of the data are shown in Figure 6(c) and (d), with the distributions of the data shown twice; shifted by the trend to 2016 levels and 1920 levels.

The return time of the OND 2016 event in Marsabit, in the NW, is about 12 years (95% CI: 3–70 years) and the trend is not significant. The best estimate of the GPD fit for the return time of the 2016 event (January–December) in Lamu, in the SE region, is about 2000 years, but the GPD does not fit the tail of the distribution very well. The lower bound of the return time of 120 years would be a better estimate for the occurrence of an event like this, given the limited amount of data. This time series shows a trend towards more precipitation (a ratio between the return times of 2016 and 1920 of at most 0.4): in 1920 the return period was about 50 years (95% CI: 5–150 years).

5.2. Return times in gridded observations

The return times of the CenTrends-ext data, shifted to 2016 and 1920 levels, are shown in Figure 7. The return time of the OND 2016 event in NW region is about 3 years (95% CI: 1–9 years) and there is no significant trend. The area-averaged drought is somewhat less extreme than the drought measured by station data. For the SE region, the return time of the 2016 January–December

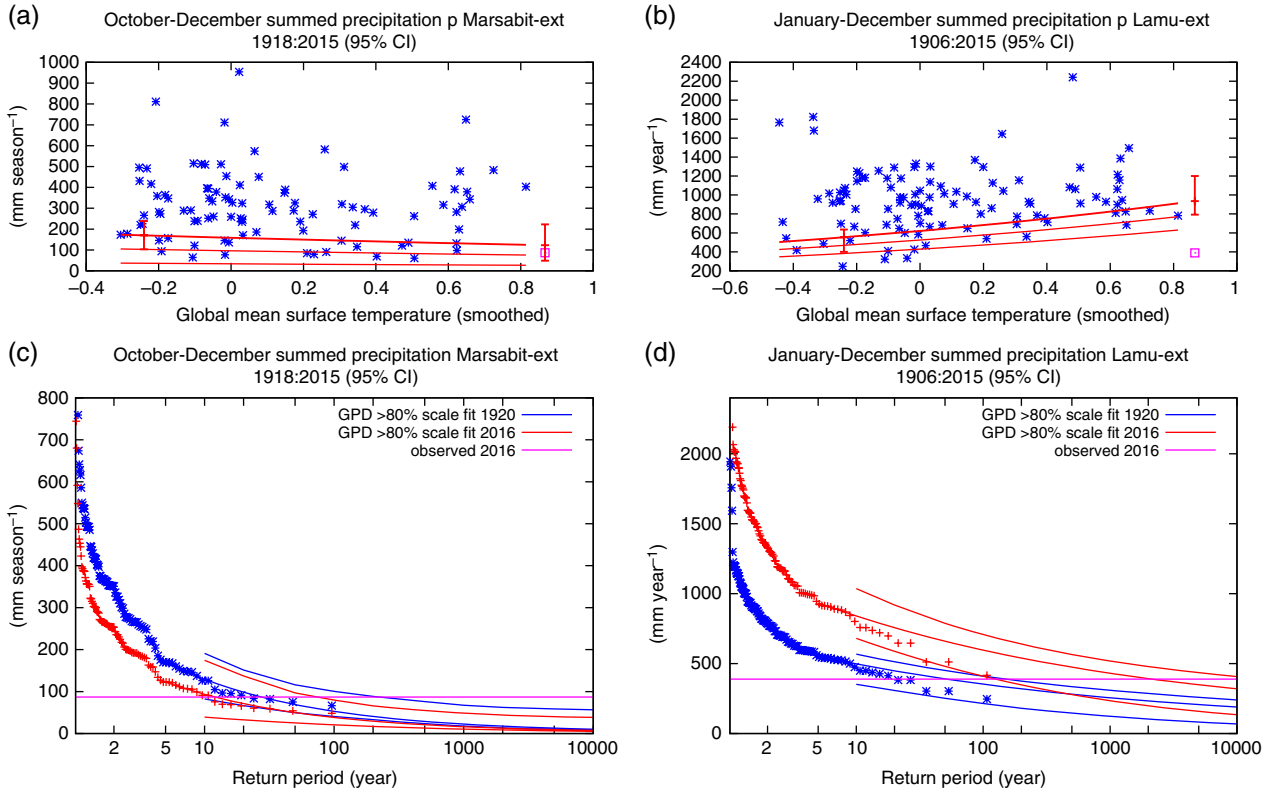

Figure 6. Precipitation station data averaged over OND (Marsabit) or January–December (Lamu). (a) and (b) are precipitation anomalies plotted against the change in global mean temperature (smoothed) for Marsabit and Lamu, respectively. The thick red line denotes the time-varying mean of the data used in the GPD fit (lowest 20%) and the thin lines are 1σ and 2σ below, respectively. The purple square shows the 2016 value, which was not used in the fit, and the two vertical red lines show the 95% confidence interval of μ for the climates of 1920 and 2016. (c) and (d) show the return periods for the data for Marsabit and Lamu, respectively. The data are shown twice, shifted to the climate of 2016 with the fitted trend (red signs) and shifted to 1920 (blue signs). Lines representing the GPD and 95% confidence interval of the GPD are also shown for the 2016 climate (red lines) and the 1920 climate (blue lines). The observed value in 2016, not used in the fit, is shown as a horizontal purple line.

precipitation was about 5 years (95% CI: 2–21 years), with no significant trend. This is much less extreme than in the station data of Lamu. From Figures 1(a) and (b), we see that the Lamu station is in the driest part of the SE region, so we expected the area average to be less extreme than in the station data. Lamu is one of the worst-affected areas, although this station might not be representative for the whole region due to coastal influence or the patchy nature of this drought.

In general, precipitation in Kenya in OND is positively correlated with El Niño, which means that in an El Niño year we expect more rain. As in 2016 we experienced La Niña conditions, we expect this season to be drier than under normal conditions. There is also a strong correlation between precipitation and Indian Ocean SSTs (WIO and DMI), especially in OND. The MAM precipitation is not correlated significantly with either NINO3.4 or Indian Ocean SSTs in the NW or SE of Kenya.

For the NW region, the variance explained by NINO3.4 in OND is 16%. When we subtract the influence of NINO3.4 linearly from the logarithm of monthly precipitation, the OND average precipitation in 2016 in an ENSO-neutral year would have been 0.89 mm day^{-1} instead of 0.62 mm day^{-1}. In OND, the WIO explains 45% of the variance in NW Kenya precipitation, and subtracting the influence of WIO (detrended with GMST) the average precipitation would have been 0.95 mm day^{-1}. Here we have not disentangled the influence of WIO and NINO3.4 but point out that ENSO may be acting through its teleconnection with the Indian Ocean. We calculated the return time of the 2016 event as if it had happened under these neutral ENSO conditions. This would have been a relatively normal year, with a return period of 2 years (95% CI: 1–3). We conclude that indeed, La Niña and the Indian Ocean SSTs caused the difference between a normal year and a dry year.

In the SE region the correlation with NINO3.4 is especially high in SON, where it explains about 17% of the variance. Because the correlation during the rest of the year is lower or not significant, the variance explained by NINO3.4 over the whole year is slightly lower, about 14%. When we subtract the influence of NINO3.4 from precipitation, the yearly average precipitation is 2.0 mm day^{-1} instead of 1.9 mm day^{-1} (also 2.0 mm day^{-1} with WIO influence subtracted, which explains 3% of the variance in precipitation). We also calculate the return time of the 2016 event in this region if it had happened under normal ENSO conditions. It would have been a relatively dry year even under normal conditions, with a return period of about 4 years (95% CI: 2–11).

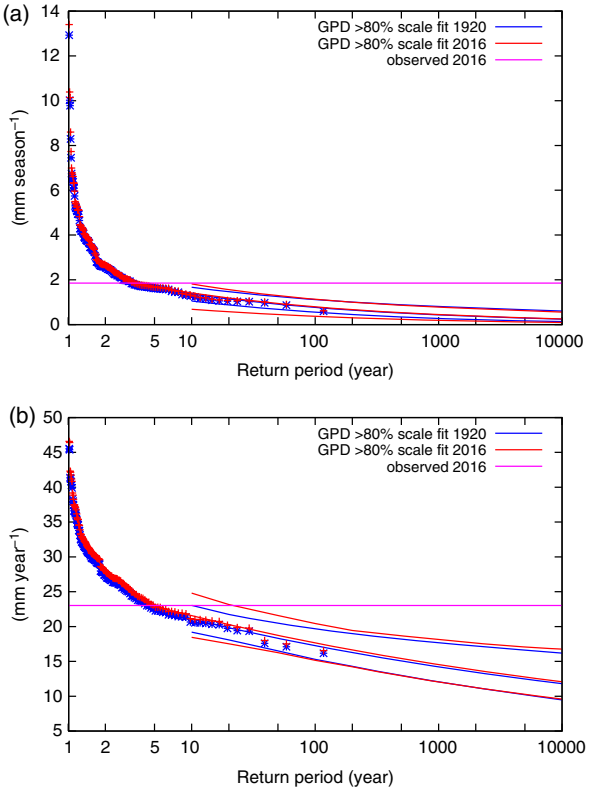

Figure 7. Same as for Figures 6(c) and (d) but for CenTrends-ext data averaged over (a) NW Kenya for OND averages and (b) SE Kenya for January–December averages.

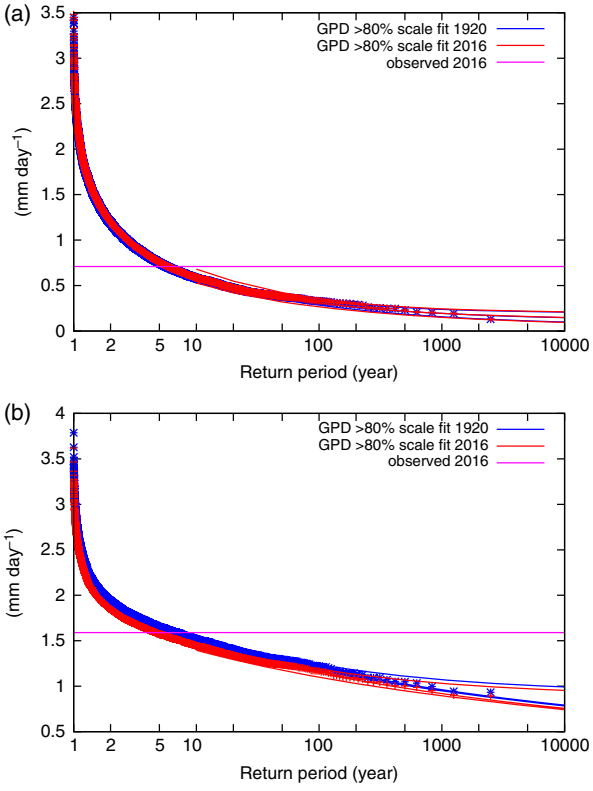

Figure 8. Same as for Figures 6(c) and (d) but for EC-Earth model data averaged over (a) NW Kenya for OND averages and (b) SE Kenya for January–December averages.

5.3. Comparison with 2010–2011 drought

As an indication of the relative severity, we compare the precipitation in the 2016 drought with the October–June 2010 drought, which caused widespread famine. In Marsabit, the return period of OND 2010 was 11 years (95% CI: 3–40), compared to 12 years in 2016. So the 2016 drought is comparable to the OND part of the 2010–2011 drought, at this specific station.

In Lamu, the dry season October 2010–June 2011, had a return period of 80 years (95% CI: 5–400 years), compared to greater than 120 years in January–December 2016. However, in this fit the year 2016 is used as well, which makes the trend towards more rainfall not significant, highlighting the sensitivity of this analysis as the fit only includes the driest 20% years. Also, considering that we are comparing two different periods (October 2010–June 2011 and January–December 2016) and that the estimate of the 2016 drought is not very well-defined for this specific station, we are not able to rank these droughts with confidence.

For the CenTrends-ext data in the NW, the return period for OND 2010 was about 60 years (95% CI: 4–180 years), compared to 3 years in 2016. So over this area, the 2016 drought was not unusual and the OND part of the 2010–2011 drought was much worse. In the SE, October 2010–June 2011 had a return period of at least 50 years. So this 2010–2011 drought was much worse than the January–December 2016 drought with a return period of 5 years, although we have to keep in mind that these consider different seasons.

From this analysis, we conclude that the 2010–2011 drought was more severe than the 2016 drought on the larger scale (in the gridded CenTrends-ext data set), however, this does vary from place to place. For example, Marsabit experienced conditions in 2016 similar to 2010–2011, and Lamu was especially dry in 2016, although the return period was not easily comparable to 2010–2011.

5.4. Global climate model analysis

Return periods for the GCMs EC-Earth and HadGEM3-A were calculated using GPD fits for the OND season in the NW and January–December in the SE, as per the observations. Values for the multiplicative bias correction are given in Table 1.

In EC-Earth, the 2016 OND event in the NW had a return period of about 6 years (95% CI: 4–9 years) (see Figure 8(a)). There is no significant trend in the model. The correlation of OND precipitation in NW Kenya with the detrended NINO3.4 index in EC-Earth is very low so we are not able to calculate the influence of El Niño in this region.

Results for the SE in EC-Earth, indicate a return period of the January–December 2016 event of about 5 years (95% CI: 4–5 years) (see Figure 8(b)). In this region we see a small trend towards less precipitation: the ratio

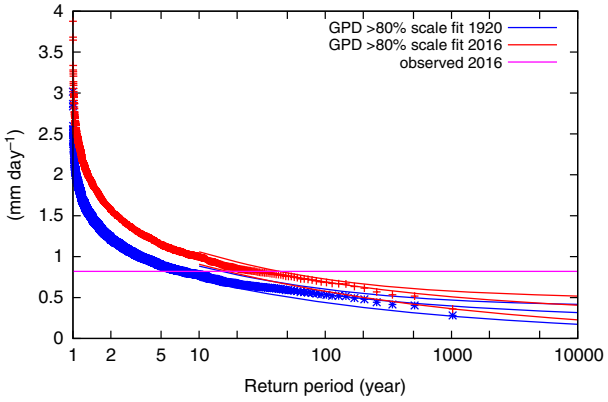

Figure 9. Same as for Figure 6(c) but for HadGEM3-A model data averaged over NW Kenya for OND averages.

between 2016 and 1920 is 1.4 (95% CI: 1.1–2.1). This means that in 1920 such an event would have happened every 7 years instead of roughly every 5 years now.

The variance of SE Kenya precipitation explained by the detrended NINO3.4 index in EC-Earth is about 10%, which is comparable to that in CenTrends-ext data. We therefore calculate the return time of the January–December 2016 precipitation value in which the influence of NINO3.4 is subtracted, similar to the analysis done in observations, with a multiplicative bias correction. If the influence of La Niña is subtracted, this increases the rainfall, resulting in an event with return period of 3 years (95% CI: 3–4 years) instead of 5 years.

In the HadGEM3-A model, our results for the NW indicate a return period of the 2016 OND event of about 33 years (95% CI: 17–44 years) (see Figure 9). In this region we see a small trend towards more precipitation: the ratio between 2016 and 1920 is 0.23 (95% CI: 0.12–0.72). This means that in 1920 such an event would have happened every 8 years (95% CI: 5–15 years) instead of once every 33 years now.

The variance explained by the detrended NINO3.4 index in OND is about 10%, which is slightly lower than in CenTrends data. We calculate the return time of the OND 2016 precipitation value in which the influence of the detrended NINO3.4 is subtracted, similar to the analysis done in observations, with a multiplicative bias correction. Without La Niña, the event would have a magnitude that occurs once in 5 years (95% CI: 3–5 years), so would not be particularly exceptional.

5.5. weather@home analysis

Figure 10 shows the weather@home distributions of precipitation for the two regions. These consistently show that the 2016 simulations are drier than the climatology, which can mainly be attributed to the SSTs (e.g. La Niña) that occurred in 2016 compared to the average year. In addition, the Actual 2016 simulations are slightly wetter than the Natural 2016 in the NW for OND, indicating that this event may have been made less likely due to climate change.

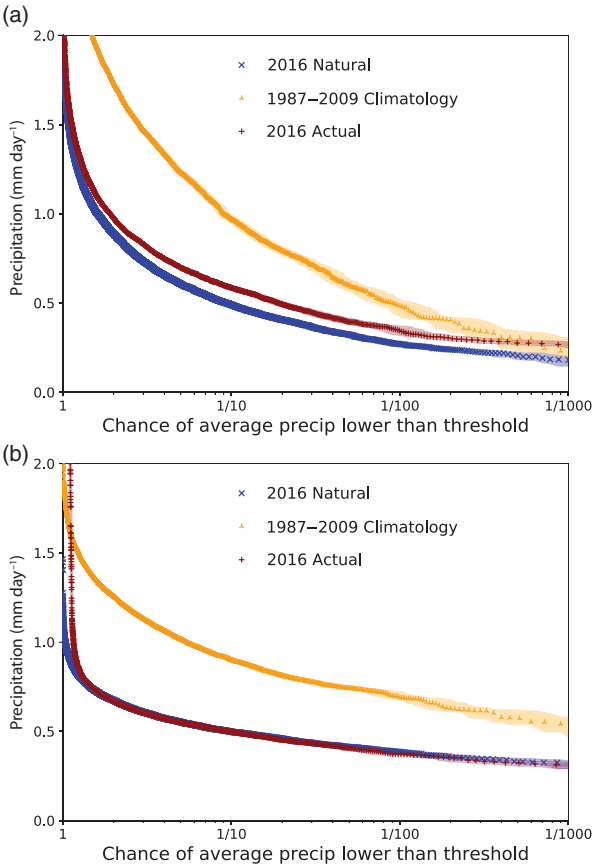

Figure 10. Return periods for precipitation in the weather@home model: (a) NW Kenya in OND, (b) SE Kenya in January–December. For each panel, three distributions are shown: Actual 2016 (red), Natural 2016 (blue), and Climatology 1987–2009 (orange). Five to 95% confidence intervals from sampling error are shown by shading.

To quantify the changes in return time in the weather@home model, we use the return time from the CenTrends-ext data set to define the event. From Section 5.2, the CenTrends-ext 2016 precipitation had return periods of 5 and 3 years, respectively, in the SE for January–December and NW for OND.

To determine the change in likelihood due to anthropogenic influence, we take the distribution from the Actual 2016 simulations as a reference and see how they changed from the Natural 2016 simulations, for the 1 in 5-year event in the SE and 1 in 3-year event in the NW. The 1 in 5-year occurrence of yearly rainfall in the SE is not changed between the 2016 Actual and 2016 Natural simulations. The event in the NW has become less likely due to climate change in the OND season, with a ratio between Actual and Natural simulations of 0.76 (CI: 0.71–0.81). We also note that the event has become also less likely due to climate change in the SE for the OND season, compensated by an increase of probability of drought in the MAM season (not shown). This indicates that human-induced warming is influencing the seasons differently, as found by Lott *et al.* (2013).

By comparing the return times between the climatology and Actual 2016 simulations, we see the effect of

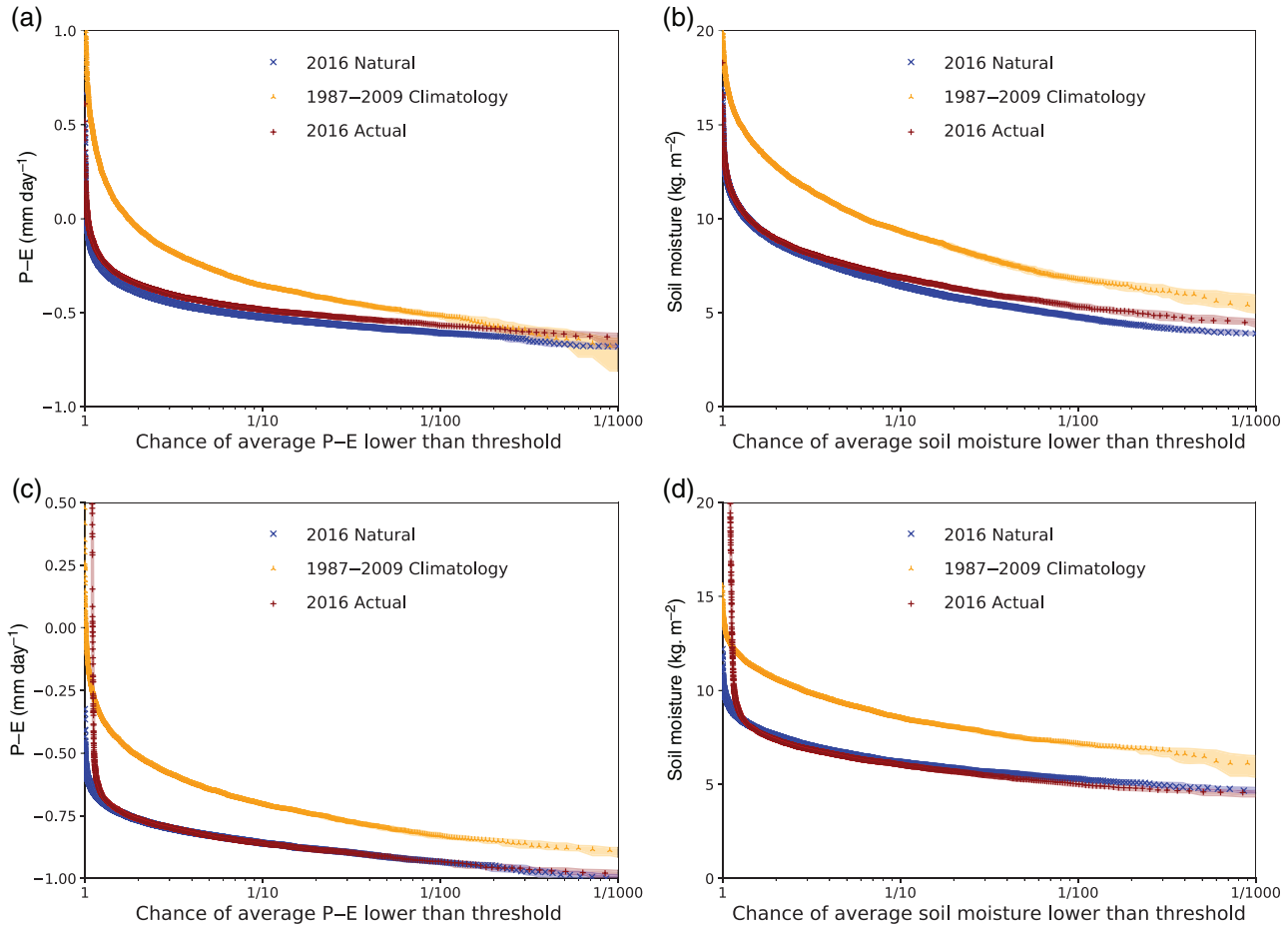

Figure 11. Return time plots of weather@home simulations as per Figure 10 but for P−E in mm day^{-1} (a and c) and soil moisture in the top 10 cm in kg m^{-2} (b and d). Upper panels are for the NW region in OND and lower panels are for the SE region in January–December.

the SST patterns of 2016 compared to a normal year. For the SE, we take the 1 in 5-year threshold in the climatology simulations. This event occurs most years with the SSTs in Actual 2016, at least four times more likely (CI: 4.06–4.64). In OND in the NW, an event that occurs 1 in 3 years in the climatology simulations, occurs most years in the Actual 2016 simulations and is at least 2 times as likely (CI: 2.50–2.75). The event was thus mainly caused by the SST patterns observed during OND 2016 which include La Niña and IOD.

The correlation of precipitation in Kenya with SST indices (DMI for Indian Ocean dipole and detrended NINO3.4 for ENSO) is strong in the OND season, with the DMI better correlated than NINO3.4 or WIO. These are based on 3-month means against OND precipitation, for 1987–2009 weather@home climatology simulations. For precipitation in the SE, NINO3.4 explains 29% of the variance in OND whereas the DMI explains 40% of the variance. The correlations are not so strong in the NW, with NINO3.4 explaining 4% of the variance or the DMI explaining 21% of the variance. Teleconnections between the different regions mean the indices are not independent, but this shows the Indian Ocean SSTs are more closely linked to Kenyan OND precipitation than Pacific SSTs in this model.

We note that for OND 2016, the DMI was −0.5 (from the OSTIA SSTs forcing the weather@home model), whereas the NINO3.4 was −1.1. We also looked at lags in the correlation between the SST indices and the weather@home precipitation and found that the 1–2-month lagged NINO3.4 has a slightly greater correlation for SE region precipitation but for all other cases (DMI and NINO3.4 for NW Kenya) the current SST indices correlated higher than the index from the previous months.

6. Other factors in the 2016 drought

Although there is no clear evidence as to the anthropogenic effects on the Kenyan precipitation in this drought, other factors such as temperature can play an important role. For example, higher temperatures may result in an increase in evapotranspiration and reduce moisture availability, impacting negatively on agriculture and worsening the effects of the drought. In the OND season of 2016, the NE was 0.8 °C and the SE was 0.7 °C above normal (using the MERRA data set, compared to 1981–2010). These higher temperatures have been reported in connection with drier conditions and lower expected crop yields (e.g. FEWSNet, 2017a).

To investigate a connection between higher temperatures and moisture availability, we conducted an examination of additional variables in the weather@home simulations. Specifically, we looked at the net precipitation minus evaporation (P – E) and soil moisture in the top 10 cm of soil.

Firstly, we note that the simulations indicate a shift of the temperature distribution in the Actual 2016 simulations, compared to the Natural 2016 simulations, as expected due to climate change. The Actual 2016 simulations were also warmer than in the Climatology simulations, relating to the particular conditions of 2016 (not shown). However, return time plots of P – E and soil moisture (Figure 11) show the same trend as the precipitation with there being slightly more moisture in the Actual 2016 simulations compared to the Natural 2016 simulation, and the Climatology simulations being wetter. This can be explained by the precipitation limiting the moisture supply – if there is no precipitation, there cannot be much additional evaporation. We do additionally note that due to the biases in the precipitation we do not quantify the change in return periods for these variables compared to the climatology.

We see that in the weather@home model, the moisture availability is dominated by the precipitation and not decreased significantly due to temperature effects for the 2016 OND season in the NW and January–December 2016 in the SE. However, as we do not have long time series of measurements of variables such as soil moisture or evaporation, we cannot easily evaluate the model performance for these quantities. The model does have biases in precipitation, and there may be influences of temperature on water availability that the model does not capture well, such as the effect on water storages or irrigated plots.

This analysis is a probe into possible factors impacting the drought other than precipitation; however, without corroborating evidence from other methods, we do not make any strong conclusions based on these results. On the other hand, we consider that higher temperatures would also be expected to increase water demand and stress on livestock (Rojas-Downing *et al.,* 2017). So even without a reduction in water availability, the effects of a drought in a warming world may be exacerbated for specific industries. This is a complicated system though, and there are also possible opposing effects such as reductions in stomatal conductance due to increased CO_2 levels acting to reduce evapotranspiration. Only an attribution study integrated with a realistic impact model will be able to draw firm conclusions.

7. Conclusions

The low precipitation of the 2016 Kenyan drought in the gridded observational data sets were not particularly extreme in the regions analysed, with return periods of 5 years (SE, January–December) and 3 years (NW, OND). However, the 2016 rainfall deficit at the specific stations we looked at was more extreme. In Lamu, an event as observed in 2016 is expected to occur less than once in 120 years and in Marsabit around once in 12 years. This indicates that although the 2016 event may not appear to be an extremely dry year over the spatial average of rainfall, individual locations may have had little to no rain.

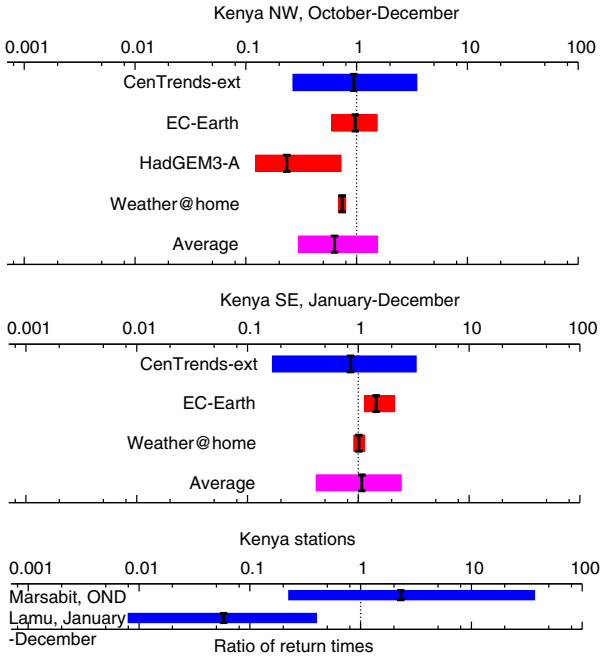

Figure 12. Synthesis showing the range of possible values for the ratio of return times between climate of 2016 and 1920 (or Natural climate for weather@home). The upper plots are gridded data sets for OND in NE Kenya, middle plots are gridded data sets for January–December in SE Kenya, and the lower plots are the station observations. The average ratios across the methods are also shown for each region, these are simple averages weighting each method equally. Observations are shown in blue, models in red and the average in purple.

There is no detectable change in the likelihood of low rainfall like the drought event observed during the 'short rain' period in 2016 in the NW of Kenya and over the annual mean of 2016 in the SE region in Kenya. Models confirm this, suggesting that anthropogenic climate change did not result in a significant trend in such a drought event. We show the spread of the possible ratios of return times between 2016 and pre-industrial in Figure 12. In these plots, a ratio of 1 represents no change due to climate change, less than 1 means the event has become less likely due to climate change (a wetting trend), and greater than 1 means the event has become more likely due to climate change (a drying trend). The trends due to climate change were not significant for the majority of methods considered. The averages (calculated from the gridded observations and climate models) are consistent with 1 (no change).

In comparison to anthropogenic climate change, the year to year variability of rainfall due to factors such as ENSO has a large influence on a drought like this. The year 2016 was a La Niña year, which is correlated with lower rainfall in Kenya in the OND season. In terms of variance of rainfall explained by the NINO3.4 index, this is 16% in the NW (OND) and 14% in the SE for

the CenTrends-ext data set (January–December). If the influence of ENSO on the rainfall deficit is subtracted from the 2016 event, this results in estimated rainfall of 0.89 mm day^{-1} instead of the observed 0.62 mm day^{-1} in the NE and 2.0 mm day^{-1} instead of 1.9 mm day^{-1} in the SE. So the hypothetical event with neutral ENSO conditions would have occurred slightly more frequently, every 2 years in the NW and every 4 years in the SE. The models that correctly reproduce the effects of La Niña show comparable results. The weather@home ensemble studies the effect of global SSTs on the probability of drought, and finds that it is made two (NW) to four (SE) times more likely by these SSTs.

The SST patterns, including the pattern associated with La Niña, did increase the likelihood of this drought. Seasonal forecasts now have some skill in predicting ENSO months ahead, and hence can give advance warning of the likelihood of low rainfall. This information is already available in the form of seasonal outlooks provided by the Kenya Meteorological Department for each rainy season; this study highlights the benefits of using this information to determine the likelihood of drought conditions. Increasing the quality and informed use of forecast data can be very useful in reducing impacts of droughts. If governments, aid organizations, and the general population can make decisions knowing the likelihood of drought conditions, they may be able to prevent or at least reduce such high levels of food insecurity.

Precipitation is not the only relevant variable though, and higher than normal temperatures in 2016 might have accelerated forage and water depletion across most of the pastoral and marginal agricultural areas (FEWSNet, 2017b). This additional stressor has increased due to climate change and will have implications during future extreme heat and drought events, as well as for livelihood activities such as crop production. The lack of significant climate change signal for precipitation in the areas studied highlights the importance of planning for the large year-to-year variations in climate. In addition, the dominant influence of predictable climate patterns, such as La Niña, during the 2016–2017 drought implies a high potential for using forecasts to trigger preventative actions, before the onset of the meteorological event.

To conclude, there is no detectable change in the likelihood of low rainfall like the drought in 2016, due to anthropogenic climate change, as observed in the short rains in NW Kenya and yearly rainfall in SE Kenya. We do note that the timing of rainfall events is also important for agriculture. This study investigated change in seasonal averaged rainfall, but it is also possible that there are changes in timing, frequency, and duration of rainfall events within a season due to climate change. Further investigation into changes to rainfall over shorter time scales, and using impact models will be beneficial in future studies.

Acknowledgements

This study was conducted as part of the Raising Risk Awareness project and the World Weather Attribution activity coordinated by Climate Central. We would like to thank the Kenya Meteorological Department for supplying their observational data. For their technical expertise, we would like to thank our colleagues at the Oxford eResearch Centre: A. Bowery, M. Rashid, S. Sparrow and D. Wallom, and the Met Office Hadley Centre PRECIS team for their technical and scientific support for the development and application of weather@home. weather@home simulations were simulated using computing resources from the AWS Cloud Credits for Research program. This work was supported by the EUCLEIA project, funded by the European Union's Seventh Framework Programme [FP7/2007-2013] under grant agreement no. 607085.

References

Ashok K, Guan Z, Yamagata T. 2003. A look at the relationship between the ENSO and the Indian Ocean dipole. *J. Meteorol. Soc. Jpn.* **81**(1): 41–56. https://doi.org/10.2151/jmsj.81.41.

Black E. 2005. The relationship between Indian Ocean sea-surface temperature and East African rainfall. *Philos. Trans. R. Soc. Lond. A* **363**(1826): 43–47. https://doi.org/10.1098/rsta.2004.1474.

Black E, Slingo J, Sperber K. 2003. An observational study of the relationship between excessively strong short rains in coastal East Africa and Indian Ocean SST. *Mon. Weather Rev.* **131**: 74–94. https://doi.org/10.1175/ 1520-0493(2003)131 ⟨0074:AOSOTR⟩2.0.CO;2.

Christidis N, Stott PA, Scaife AA, Arribas A, Jones GS, Copsey D, Knight JR, Tennant WJ. 2013. A new HadGEM3-A-based system for attribution of weather- and climate-related extreme events. *J. Clim.* **26**(9): 2756–2783. https://doi.org/10.1175/JCLI-D-12-00169.1.

Coles S. 2001. *An Introduction to Statistical Modeling of Extreme Values*. Springer Series in Statistics. Springer-Verlag: London, 208 pp.

Donlon CJ, Martin M, Stark J, Roberts-Jones J, Fiedler E, Wimmer W. 2012. The operational sea surface temperature and sea ice analysis (OSTIA) system (Advanced Along Track Scanning Radiometer(AATSR) Special Issue). *Remote Sens. Environ.* **116**: 140–158. https://doi.org/10.1016/j.rse.2010.10.017.

FEWSNet. 2017a. *East Africa seasonal monitor*. http://www.fews.net/sites/default/files/documents/reports/EA_Seasonal%20Monitor_2017_01_06.pdf (accessed 30 March 2017).

FEWSNet. 2017b. *Pastoral areas to experience worst food insecurity outcomes as the dry season progresses*. http://www.fews.net/east-africa/kenya/key-message-update/january-2017 (accessed 30 March 2017).

Fischer AS, Terray P, Guilyardi E, Gualdi S, Delecluse P. 2005. Two independent triggers for the Indian Ocean dipole/zonal mode in a coupled GCM. *J. Clim.* **18**(17): 3428–3449. https://doi.org/10.1175/JCLI3478.1.

Funk C, Husak G, Michaelsen J, Shukla S, Hoell A, Lyon B, Hoerling MP, Liebmann B, Zhang T, Verdin J, Galu G, Eilerts G, Rowland J. 2013. Attribution of 2012 and 2013–12 rainfall deficits in eastern Kenya and southern Somalia [in "explaining extremes of 2012 from a climate perspective"]. *Bull. Amer. Met. Soc.* **94**(9): S45–S48.

Funk C, Nicholson S, Landsfeld M, Klotter D, Peterson P, Harrison L. 2015a. The centennial trends greater horn of Africa precipitation dataset. *Dryad*. https://doi.org/10.5061/dryad.nk78.

Funk C, Peterson P, Landsfeld M, Pedreros D, Verdin J, Shukla S, Husak G, Rowland J, Harrison L, Hoell A, Michaelsen J. 2015b. The climate hazards infrared precipitation with stations – a new environmental record for monitoring extremes. *Sci. Data* **2**(150): 066. https://doi.org/10.1038/sdata.2015.66.

Goddard L, Graham NE. 1999. Importance of the Indian Ocean for simulating rainfall anomalies over eastern and southern Africa. *J. Geophys. Res.* **104**(D16): 19099–19116.

Hauser M, Gudmundsson L, Orth R, Jézéquel A, Haustein K, Vautard R, van Oldenborgh GJ, Wilcox L, Seneviratne SI. 2017. Methods and model dependency of extreme event attribution: the 2015 European drought. *Earth's Future* **5**: 1034–1043. https://doi.org/10.1002/2017EF000612.

Hazeleger W, Severijns C, Semmler T, Ştefănescu S, Yang S, Wang X, Wyser K, Dutra E, Baldasano JM, Bintanja R, Bougeault P, Caballero

R, Ekman AML, Christensen JH, van den Hurk B, Jimenez P, Jones C, Kållberg P, Koenigk T, McGrath R, Miranda P, van Noije T, Palmer T, Parodi JA, Schmith T, Selten F, Storelvmo T, Sterl A, Tapamo H, Vancoppenolle M, Viterbo P, Willén U. 2010. EC-Earth: a seamless earth-system prediction approach in action. *Bull. Amer. Meteor. Soc.* **91**(10): 1357–1363. https://doi.org/10.1175/2010BAMS2877.1.

Hoell A, Funk C, Barlow M. 2014. La Niña diversity and northwest Indian Ocean rim teleconnections. *Clim. Dyn.* **43**(9): 2707–2724. https://doi.org/10.1007/s00382-014-2083-y.

Hoell A, Hoerling M, Eischeid J, Quan X-W, Liebmann B. 2017. Reconciling theories for human and natural attribution of recent east Africa drying. *J. Clim.* **30**(6): 1939–1957. https://doi.org/10.1175/JCLI-D-16-0558.1.

KFSSG. 2017. *The 2016 short rains season assessment report*. http://reliefweb.int/sites/reliefweb.int/files/resources/Kenya_2016_SRA_NationalReport.pdf (accessed 30 March 2017).

Liebmann B, Bladé I, Funk C, Allured D, Quan XW, Hoerling M, Hoell A, Peterson P, Thiaw WM. 2017. Climatology and interannual variability of boreal spring wet season precipitation in the eastern horn of Africa and implications for its recent decline. *J. Clim.* **30**(10): 3867–3886. https://doi.org/10.1175/JCLI-D-16-0452.1.

Lott FC, Christdis N, Stott PA. 2013. Can the 2011 East African drought be attributed to climate change? *Geophys. Res. Lett.* **40**(6): 1177–1181. https://doi.org/10.1002/grl.50235.

Lyon B, DeWitt DG. 2012. A recent and abrupt decline in the east African long rains. *Geophys. Res. Lett.* **39**(2): l02702. https://doi.org/10.1029/2011GL050337.

Marthews TR, Otto FEL, Mitchell D, Dadson SJ, Jones RG. 2015, 2015. The 2014 drought in the horn of Africa: attribution of meteorological studies. *Bull. Amer. Meteor. Soc.* **17**: S83–S88. https://doi.org/10.1175/BAMS-D-15-00115.1.

Massey N, Jones R, Otto FEL, Aina T, Wilson S, Murphy JM, Hassell D, Yamazaki YH, Allen MR. 2015. weather@home – development and validation of a very large ensemble modelling system for probabilistic event attribution. *Q. J. Roy. Meteor. Soc.* **141**: 1528–1545. https://doi.org/10.1002/qj.2455.

McKee TB, Doesken NJ, Kleist J. 1993. The relationship of drought frequency and duration to time scales. In *Proceedings of the 8th Conference on Applied Climatology*, Vol. 17, American Meteorological Society, Boston, MA, 179–183.

Mutai CC, Ward MN. 2000. East African rainfall and the tropical circulation/convection on intraseasonal to interannual timescales. *J. Clim.* **13**: 3915–3939. https://doi.org/10.1175/1520-0442(2000)013<3915:EARATT>2.0.CO;2.

NDMA. 2017. *National drought early warning bulletin*. http://www.ndma.go.ke/resource-center/send/39-drought-updates/4116-national-drought-early-warning-bulletin-march-2017 (accessed 30 March 2017).

Nicholson SE, Selato JC. 2000. The influence of La Nina on African rainfall. *Int. J. Climatol.* **20**: 1761–1776. https://doi.org/10.1002/1097-0088(20001130)20:14<1761::AID-JOC580>3.0.CO;2-W.

Peterson TC, Vose RS. 1997. An overview of the global historical climatology network temperature database. *Bull. Am. Meteorol. Soc.* **78**(12): 2837–2849. https://doi.org/10.1175/1520-0477(1997)078⟨2837:AOOTGH⟩2.0.CO;2.

Philip S, Kew SF, van Oldenborgh GJ, Otto F, O'Keefe S, Haustein K, King A, Zegeye A, Eshetu Z, Hailemariam K, Singh R, Jjemba E, Funk C, Cullen H. 2017. Attribution analysis of the Ethiopian drought of 2015. *J. Clim.* https://doi.org/10.1175/JCLI-D-17-0274.1.

Preethi B, Sabin TP, Adedoyin JA, Ashok K. 2015. Impacts of the ENSO Modoki and other tropical Indo-Pacific climate-drivers on African rainfall. *Sci. Rep.* **5**: 16653. https://doi.org/10.1038/srep16653.

Republic of Kenya. 2012. Releasing our full potential. Sessional paper no. 8 of 2012 on national policy for the sustainable development of northern Kenya and other arid lands, Ministry of State for Development of Northern Kenya and other Arid Lands.

Rojas-Downing MM, Nejadhashemi AP, Harrigan T, Woznicki SA. 2017. Climate change and livestock: impacts, adaptation, and mitigation. *Clim Risk Manag* **16** (suppl C): 145–163. https://doi.org/10.1016/j.crm.2017.02.001.

Rowell DP, Booth BBB, Nicholson SE, Good P. 2015. Reconciling past and future rainfall trends over east Africa. *J. Clim.* **28**(24): 9768–9788. https://doi.org/10.1175/JCLI-D-15-0140.1.

Saji N, Goswami B, Vinayachandran P, Yamagata T. 1999. A dipole mode in the tropical Indian Ocean. *Nature* **401**(6751): 360–363.

Schaller N, Otto FEL, van Oldenborgh GJ, Massey NR, Sparrow S, Allen MR. 2014. The heavy precipitation event of May–June 2013 in the upper Danube and Elbe basins [in "explaining extremes of 2013 from a climate perspective"]. *Bull. Amer. Meteor. Soc.* **95**(9): S69–S72.

Schaller N, Kay AL, Lamb R, Massey NR, van Oldenborgh GJ, Otto FEL, Sparrow SN, Vautard R, Yiou P, Ashpole I, Bowery A, Crooks SM, Haustein K, Huntingford C, Ingram WJ, Jones RG, Legg T, Miller J, Skeggs J, Wallom D, Weisheimer A, Wilson S, Stott PA, Allen MR. 2016. Human influence on climate in the 2014 southern England winter floods and their impacts. *Nat. Clim. Chang.* **6**: 627–634.

Shongwe ME, van Oldenborgh GJ, van den Hurk BJJM, van Aalst MK. 2011. Projected changes in mean and extreme precipitation in Africa under global warming. Part II: East Africa. *J. Clim.* **24**(14): 3718–3733. https://doi.org/10.1175/2010JCLI2883.1.

Stockdale TN, Anderson DLT, Balmaseda MA, Doblas-Reyes F, Ferranti L, Mogensen K, Palmer TN, Molteni F, Vitart F. 2011. ECMWF seasonal forecast system 3 and its prediction of sea surface temperature. *Clim. Dyn.* **37**(3): 455–471. https://doi.org/10.1007/s00382-010-0947-3.

Taylor K, Stouffer RL, Meehl GA. 2012. An overview of CMIP5 and the experiment design. *Bull. Amer. Meteor. Soc.* **93**: 485–498. https://doi.org/10.1175/ BAMS-D-11-00094.1.

van der Wiel K, Kapnick SB, van Oldenborgh GJ, Whan K, Philip S, Vecchi GA, Singh RK, Arrighi J, Cullen H. 2017. Rapid attribution of the August 2016 flood-inducing extreme precipitation in south Louisiana to climate change. *Hydrol. Earth Syst. Sci.* **21**(2): 897–921. https://doi.org/10.5194/hess-21-897-2017.

Yang W, Seager R, Cane MA, Lyon B. 2014. The east African long rains in observations and models. *J. Clim.* **27**(19): 7185–7202. https://doi.org/10.1175/JCLI-D-13-00447.1.